Journal of
Marine Science and Engineering

MDPI

Article

Numerical Study on Fluid Dynamic Characteristics of a Cross-Flow Fan

Xiaowei Cai *, Chun Zhang and Baoshou Wang

China Ship Scientific Research Center, Wuxi 210084, China
* Correspondence: xiaocai2601@163.com

Abstract: This paper focuses on the application of a cross-flow fan (CFF) to generate propulsion for a submersible aircraft with a flying wing configuration. A numerical method is established to simulate the CFF operating both in the air and underwater. This paper then investigates the fluid dynamic characteristics of the CFF, including the velocity field, the pressure field, the cavitation distribution, the lift, and the thrust. It is concluded that proper lifts and thrusts can be obtained when the rotating speed and the angle of attack are reasonably designed. This work provides a valuable numerical methodology for studying the fluid dynamic characteristics of the CFF operating in different media and offers a technical basis for the selection of a motor system for submersible aircraft.

Keywords: submersible aircraft; cross-flow fan; flying wing; propulsion; lift and thrust; computational fluid dynamics; flow field

1. Introduction

The submersible aircraft is a special aircraft that can both dive underwater and fly in the air, the research into which began in the 1930s. One of the original conceptual studies of submersible aircraft proposed a design that combined the speed and range of an airborne platform with the stealth of an underwater vehicle by developing a flyable and submersible vessel [1]. The challenges of producing such an aircraft mainly come from aspects including the propulsive system, the overall vehicle density, and the take-off/landing process [2]. The propulsive system of submersible aircraft has been a subject of intense interest, as it is extremely complicated to explore and characterize an integrated propulsive structure that meets the requirements of a submersible aircraft flying in the air at times and diving underwater at other times.

In 1979, Harloff [3] proposed installing a cross-flow fan (CFF) inside an airfoil to generate a propulsive wing for aircraft. Since then, numerous researchers have engaged in investigating the feasibility of such an installation. It was demonstrated that the propulsive power could be reasonably reduced by ingesting the viscous wake into an engine to smooth the wake distortion behind the body [4]. Another work proved that the drag force of the aircraft could be reduced by up to 18 to 20% by eliminating the engine pylon/nacelle support structure, thus improving the corresponding cruise efficiency and range [5]. Kummer and Dang proposed a concept of the so-called high-lift propulsive airfoil for aircraft applications [6]. In 2008, Casparie and Dang demonstrated a structure for synergistically integrating a CFF with a thick subsonic airfoil to achieve lift augmentation and thrust production [7], as shown in Figure 1. In 2003, Peebles patented a fan-wing structure and its application in a cargo plane [8], as shown in Figure 2. The investigation of CFF propulsion for lightweight vertical take-off and landing (VTOL) aircraft was proposed by Gossett [9]. The ducted propellers of the lightweight VTOL aircraft provide both lift and cruise thrust with VTOL lift augmentation from a CFF.

check for updates

Citation: Cai, X.; Zhang, C.; Wang, B. Numerical Study on Fluid Dynamic Characteristics of a Cross-Flow Fan. *J. Mar. Sci. Eng.* **2023**, *11*, 846. https://doi.org/10.3390/jmse11040846

Academic Editors: María Isabel Lamas Galdo, Abdellatif Ouahsine and Rafael J. Bergillos

Received: 15 January 2023
Revised: 27 March 2023
Accepted: 11 April 2023
Published: 17 April 2023

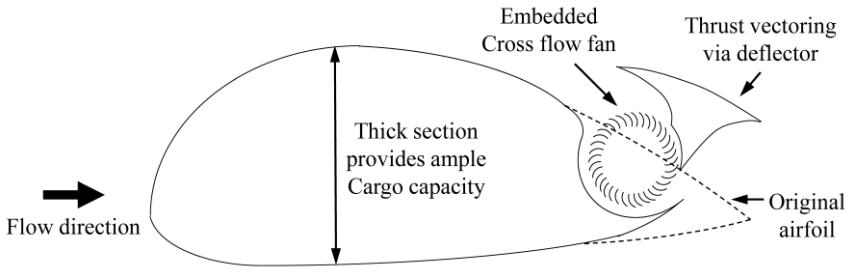

Figure 1. Propulsive airfoil concept proposed by Casparie and Dang. Adapted with permission from Ref. [7].

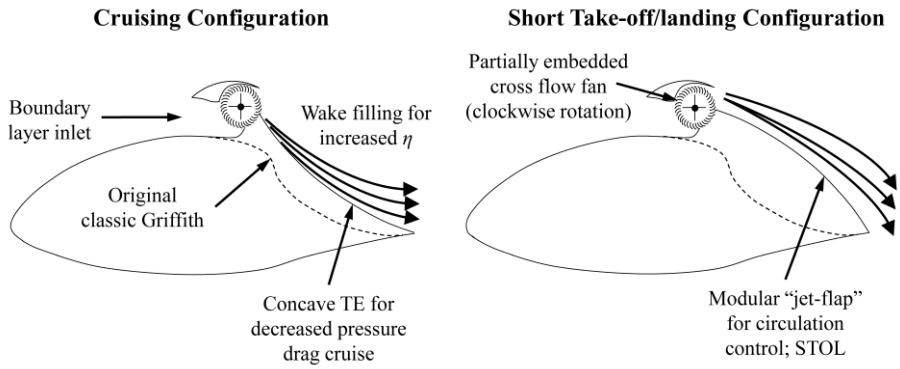

Figure 2. Cross section of the propulsion-airframe integrated CFF-airfoil design. Adapted with permission from Ref. [8].

Generally, the CFF propulsive wing has the following four application features. First, the CFF accelerates the incoming flow near the upper surface, which gives rise to a large pressure difference between the upper and the lower surfaces. Thus, the CFF configuration produces extra lift. Second, since the velocity of the jet flow is greater than that of the incoming flow, an additional thrust is thus obtained from the CFF configuration. Third, the CFF configuration, playing a role in controlling the boundary layer, can delay the flow separation. Fourth, the CFF configuration in engineering applications can be easily extended spanwise due to its two-dimensional nature. As it is a propulsion generator for an aircraft, the CFF has shown high effectiveness in both air propulsion [10] and underwater propulsion (Figure 3) [11].

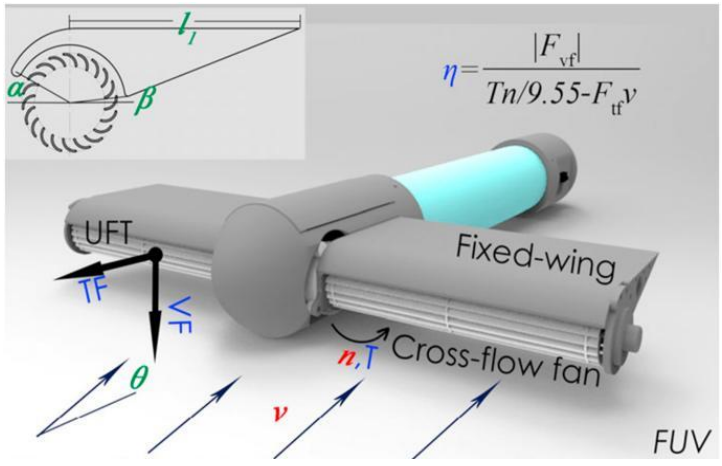

Figure 3. A diagram of a fan-wing underwater vehicle (FUV) experiment. Reprinted with permission from Ref. [11].

Although research into fan-wing airfoils is abundant [12–23], the comprehensive fluid dynamic characteristics of the CFF embedded in flying wings have still been rarely investigated. Therefore, this work proposes to utilize the CFF as the propeller of the submersible aircraft with a flying wing configuration, and the corresponding aerodynamic and hydrodynamic characteristics are thoroughly investigated using computational fluid dynamics (CFD). Importantly, two essential performance parameters, the lift and the thrust of the CFF operating in different media, are systematically studied.

2. Mathematical Model

The fluids studied in this paper are air and water. Three governing equations of fluid flows are involved in the mathematical model, including the conservation of continuity, the conservation of momentum, and the conservation of energy equations [24–26]. Assuming the flow is isothermal, the energy equation can be ignored. Hence, the flow field can be solved by only coupling the continuity Equation (1) and the momentum Equation (2).

The physical principle of the continuity equation is that mass can neither be created nor destroyed. The continuity equation in the form of a partial differential equation is given by:

$$\frac{\partial \rho}{\partial t} + \nabla \cdot \left(\rho \vec{V} \right) = 0 \tag{1}$$

where ρ is the density of the fluids and $\vec{V}$ is the fluid velocity vector, respectively. The air and the water studied in this work are considered to be incompressible. The physical principle of the momentum equation is that the force is equal to the change rate of momentum with time. The momentum equation in the form of a partial differential equation is obtained as:

$$\frac{\partial \left(\rho \vec{V} \right)}{\partial t} + \nabla \cdot \left(\rho \vec{V} \vec{V} \right) = -\nabla p + \nabla \cdot \left(\vec{\tau} \right) + \rho \vec{g} + \vec{F} \tag{2}$$

where p is the static pressure, $\vec{\tau}$ is the stress tensor, and $\rho \vec{g}$ and $\vec{F}$ are the gravitational body force and the external body force, respectively.

Air and water are assumed as Newtonian fluids. The stress tensor $\vec{\tau}$ applied in Equation (2) is given by:

$$\vec{\tau} = \mu \left[\left(\nabla \vec{V} + \nabla \vec{V}^T \right) - \frac{2}{3} \nabla \cdot \vec{V} I \right] \tag{3}$$

where μ is the molecular viscosity and I is the unit tensor.

The continuity and the momentum equations above are jointly called the Navier–Stokes equations. To solve the above equations for a turbulent flow, the principle of Reynolds averaging is applied in this paper. Taking a time average on the mean quantities will yield the Reynolds-averaged Navier–Stokes (RANS) equations:

$$\frac{\partial \rho}{\partial t} + \frac{\partial \rho}{\partial x_i} (\rho u_i) = 0 \tag{4}$$

$$\frac{\partial}{\partial t} (\rho u_i) + \frac{\partial}{\partial x_j} (\rho u_i u_j) = -\frac{\partial p}{\partial x_i} + \frac{\partial}{\partial x_j} \left[\mu \left(\frac{\partial u_i}{\partial x_j} + \frac{\partial u_j}{\partial x_i} - \frac{2}{3} \delta_{ij} \frac{\partial u_l}{\partial x_l} \right) \right] + \frac{\partial}{\partial x_j} \left(-\rho \overline{u_i' u_j'} \right) \tag{5}$$

where the term $-\rho \overline{u_i' u_j'}$ in Equation (5) is the Reynolds stress tensor. The k-ω model [27] is applied in this paper to assess the effect of turbulence.

As for the situation of a CFF operating underwater, the high rotating speed of the blades of a CFF may dramatically decrease the local flow pressure and thus lead to a cavitation phenomenon around the blades. Therefore, the Schnerr–Sauer (S-S) cavitation model is used to characterize the volume fractions of water and vapor [28]. The volume fraction of vapor, α_v, satisfies the following relation:

$$\frac{\partial \alpha_v \rho_v}{\partial t} + \nabla \cdot \left(\alpha_v \rho_v \vec{V} \right) = R_e - R_c \tag{6}$$

where the term ρ_v is the vapor density. The source terms of mass, R_e and R_c, are derived from the bubble dynamics equation and represent the evaporation term and the condensation term, respectively. They are given by:

$$R_e = \frac{\rho_v \rho_l \alpha_v (1 - \alpha_v - \alpha_g)}{\rho_m} \frac{3}{R_B} \sqrt{\frac{2\max(p_v - p, 0)}{3\rho_l}} \tag{7}$$

$$R_c = -\frac{\rho_v \rho_l \alpha_v (1 - \alpha_v - \alpha_g)}{\rho_m} \frac{3}{R_B} \sqrt{\frac{2\max(p - p_v, 0)}{3\rho_l}} \tag{8}$$

where R_B, α_g, and ρ_l are the diameter of the bubble, the volume fraction of the non-condensable gas (NCG), and the density of the liquid, respectively.

Since calculations of unsteady flow usually consume computer resources distinctively, the numerical study can be carried out by using the explicit time discretization method [29] and implicit time discretization method [30,31]. This work adopts the latter method of second-order accuracy to conduct the numerical studies.

3. Numerical Method and Models

Many influencing factors, such as rotating speeds, fluid velocities, angles of attack, opening angles of leading-edge, installation angles of the blade, airfoils, blade shapes, shell sizes, numbers of blades, fan openings, fan outlets, etc., are involved in the design and calculation of CFFs [32–35]. As for the numerical simulations, the most critical challenges are how to deal with the complex structures in different dimensions within the flow field and to efficiently exchange all the information of flow fields between the rotation region and the static region. This work proposes to segment the whole domain into two subdomains, including the rotating subdomain and the static subdomain, with considering their different features of movement and structural configuration to simplify and accelerate the calculations. In addition, the sliding interface technique is employed to realize real-time exchanges of information between the rotating subdomain and the surrounding static subdomain.

A two-dimensional numerical study is carried out first to validate the principle of the CFF and, importantly, the corresponding numerical methodology with effective technical schemes for further characteristic investigations in CFFs. Assume that the CFF operates in the air with a freestream velocity of 1 m/s, an atmospheric pressure of 101,325 Pa, and a fan speed of 3000 rpm. The software STAR-CCM+ is employed to process all the numerical calculations in this work due to its high efficiency in the mesh generation of complex simulation domains composed of multiple elements. Figure 4a below shows the overall grid system of the two-dimensional calculation domain. The center of the fan rotor is located at 80% of the chord length of the airfoil. In addition, Figure 4b shows the local grid around the CFF, which involves 26 blades. The total numbers of the grids and the nodes are 50,342 and 25,877, respectively.

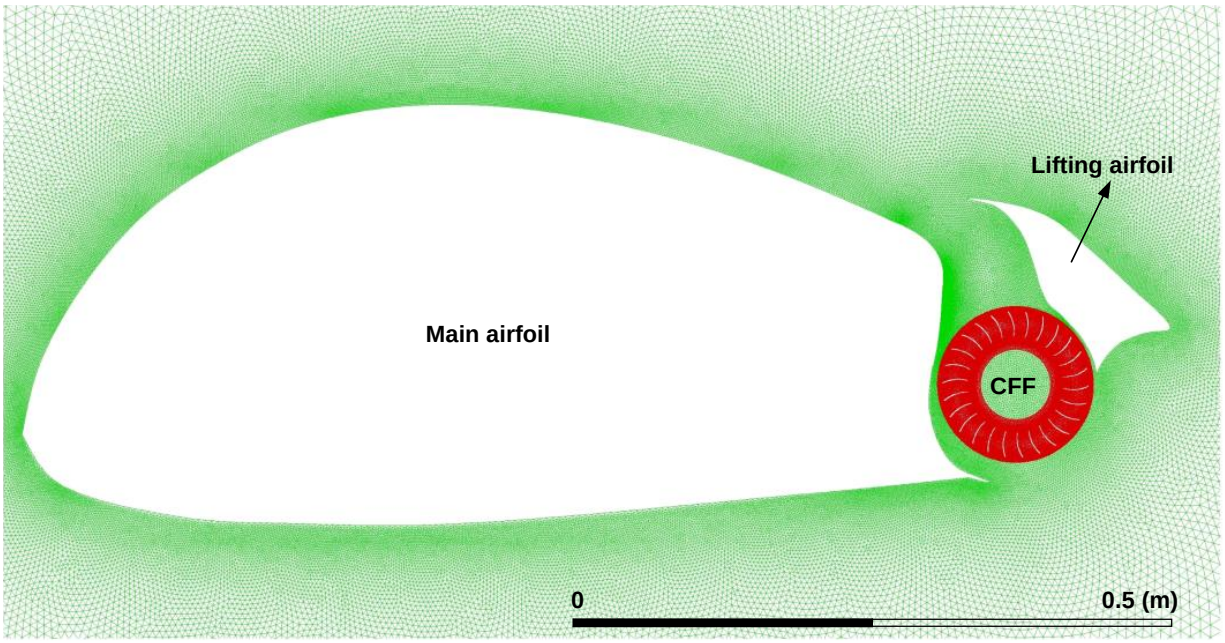

(a)

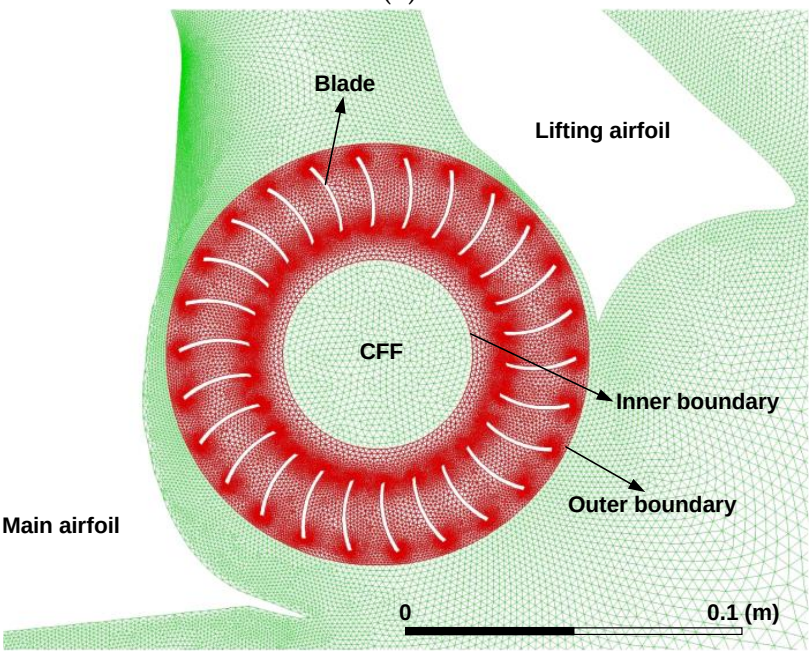

(b)

Figure 4. Grid system of the two-dimensional calculation domain: (**a**) grid system of the overall calculation domain; and (**b**) local grids inside and around the CFF.

Figure 5 shows the corresponding evolution of the velocity and the pressure fields within and around the CFF. It is seen that, due to the rotation of blades, the fluid on the upper surface of the airfoil is gradually absorbed and discharged at an accelerated rate. The velocity and the pressure on the upper and lower surfaces gradually change, and eccentric vortices are generated near the fan axis. The flow field gradually tends to be stable after 0.1 s. Therefore, the feasibility of the principle of the CFF and the corresponding numerical methodology is successfully validated.

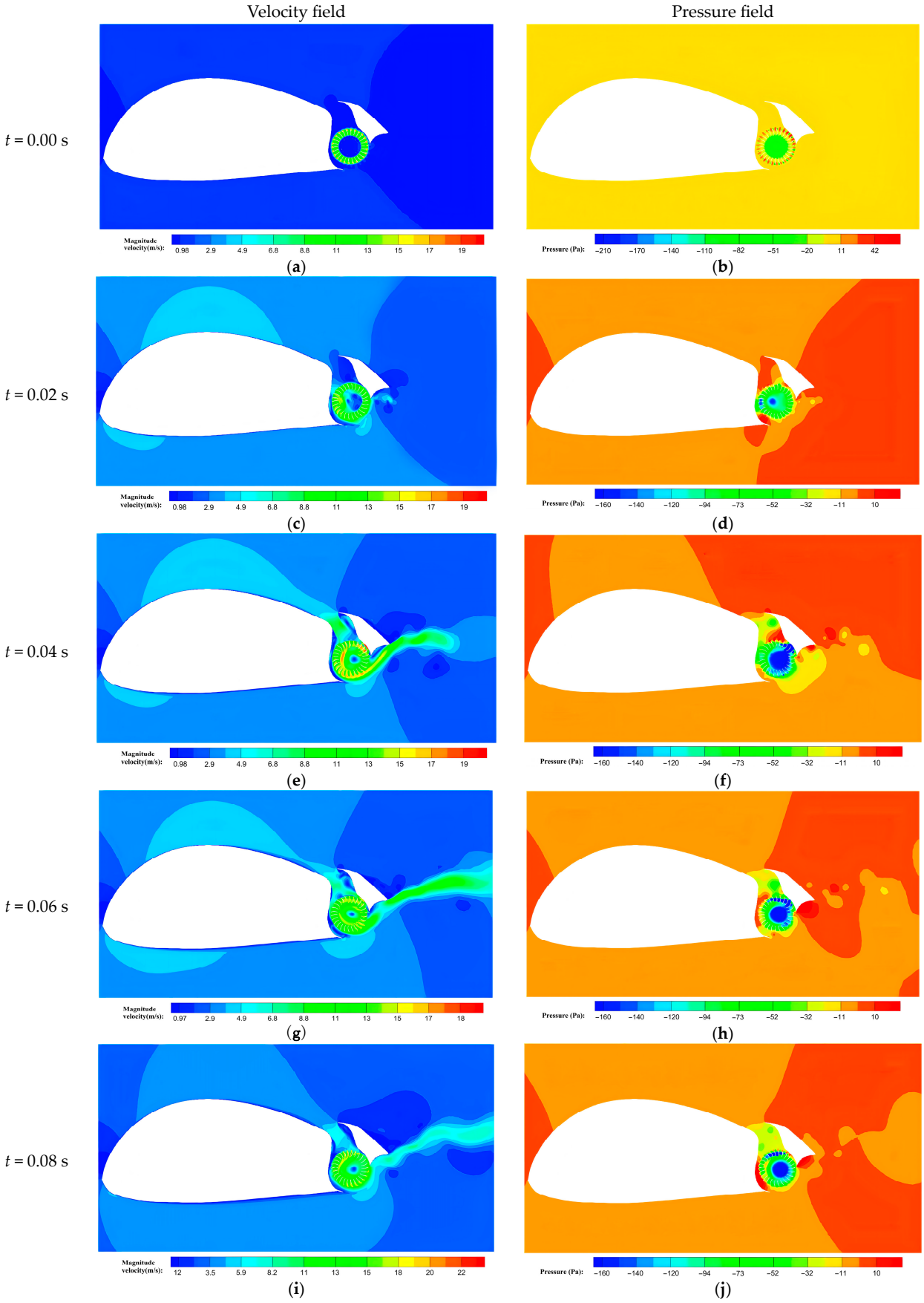

Figure 5. *Cont.*

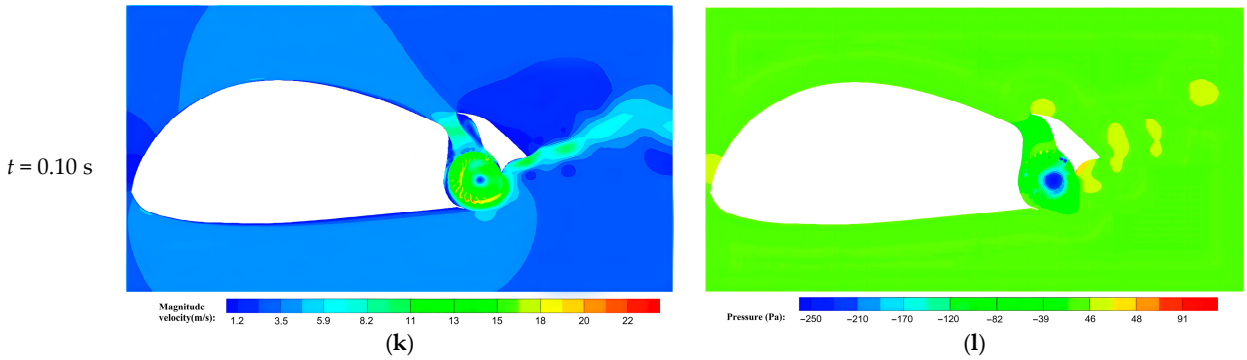

Figure 5. The evolution of the velocity and pressure fields within and around the CFF under conditions of a freestream velocity of 1 m/s, an atmospheric pressure of 101,325 Pa, and a fan speed of 3000 rpm. The subfigures in the left column indicate the evolution of the pressure from 0 s to 0.10 s. The subfigures in the right column indicate the evolution of the velocity from 0 s to 0.10 s.

To further validate the accuracy of the proposed numerical method in this paper, the results are also compared with the reported experimental data achieved from a wind tunnel [36]. Two performance parameters of the fan—fan flow coefficient $\varphi = U/\omega D$ and lift coefficient $C_l = F_l/\left(0.5\rho U^2 b\right)$—are used here to facilitate the validation, where U, ω, D, and b are the freestream velocity, the fan angular velocity, the fan diameter, and the chord length of the airfoil, respectively. Figure 6 displays the comparison of the lift coefficients at different fan flow coefficients achieved from this work and Ref. [36], which shows good consistency with a maximum error of only 8.45%.

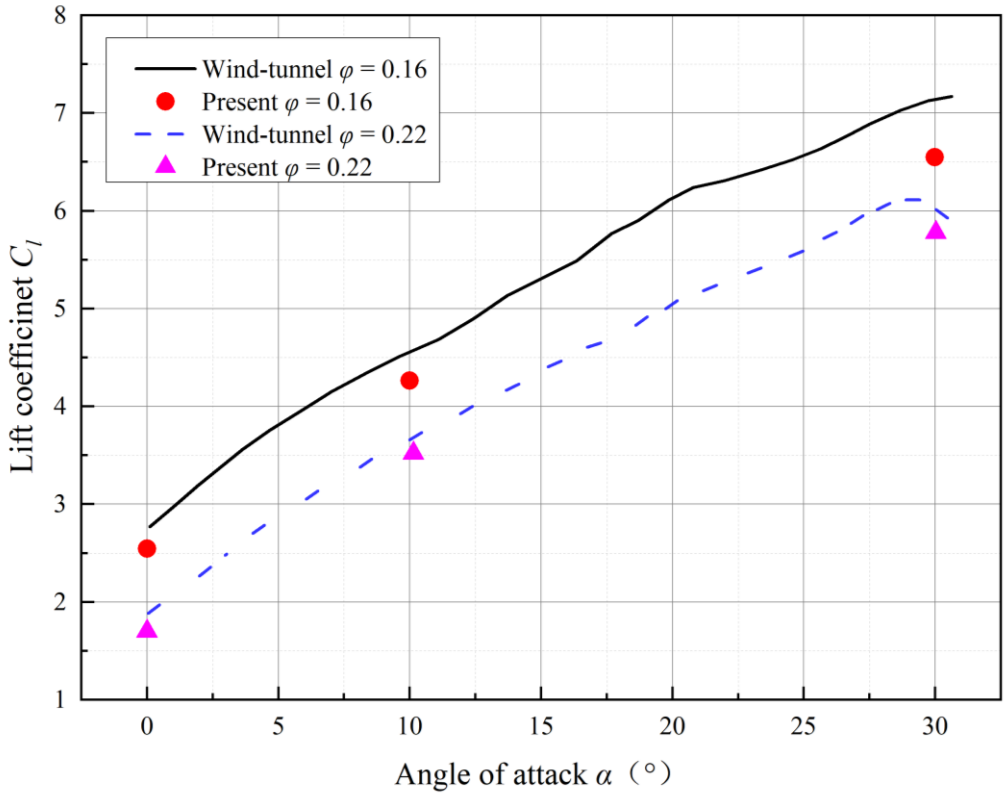

Figure 6. Validation of the numerical methodology through comparing with the reported experimental results from Ref. [36].

4. Results and Discussion

Based on the validated numerical methodology in the last section, this work consequently conducts a systematic numerical investigation of the fluid dynamic characteristics of a three-dimensional CFF (Figure 7), designed for a flying wing-type submersible aircraft. The width and length of the submersible aircraft are 3000 mm and 2400 mm, respectively. The exact position of the center of the CFF is located in the x-o-y plane with coordinates of $x = -2200$ mm and $y = 80$ mm, the number of blades of the CFF is set as 18, and the radiuses of the inner boundary and outer boundary of the blades within the CFF are 115 mm and 175 mm, respectively.

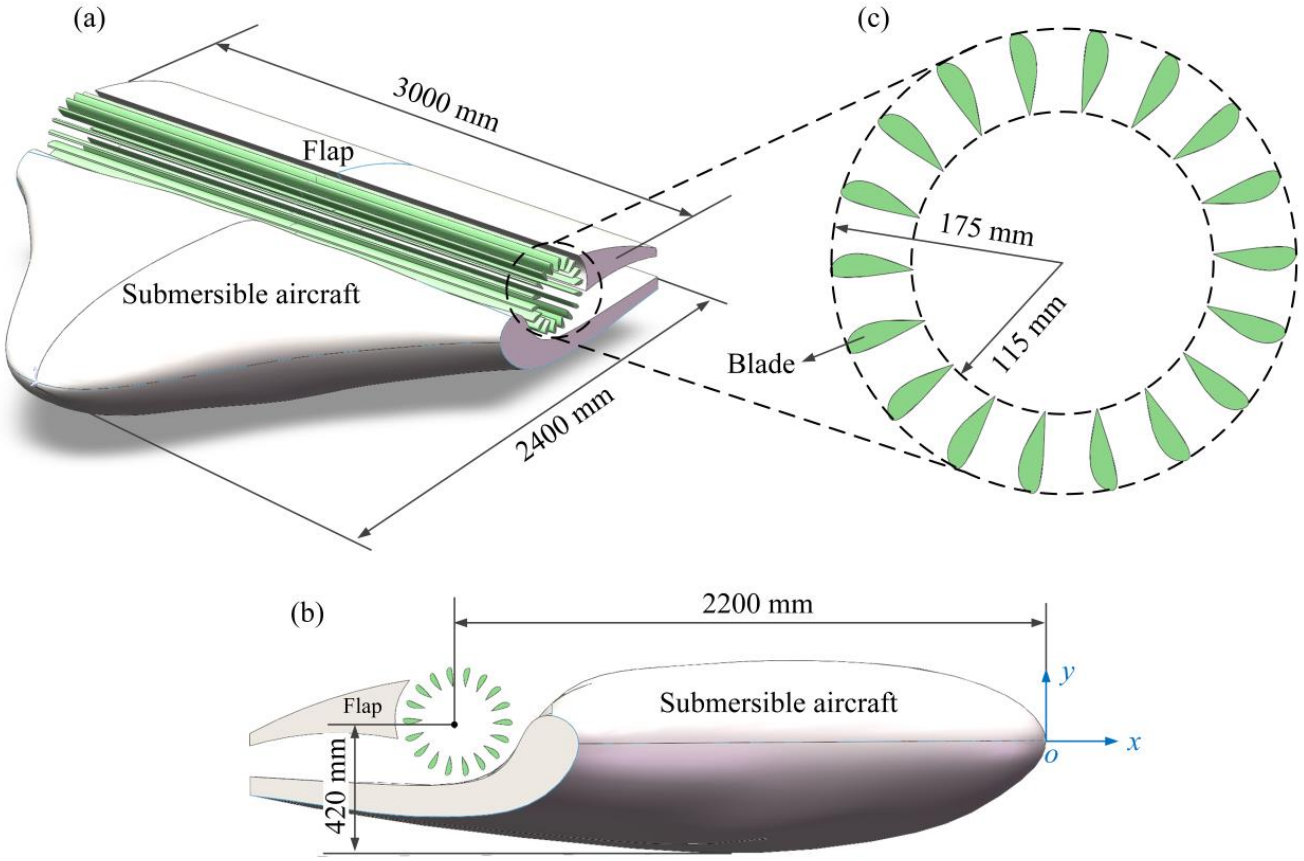

Figure 7. Schematic of a three-dimensional CFF installed in a submersible aircraft: (**a**) the overall view of the submersible aircraft; (**b**) the side view of the submersible aircraft; and (**c**) the configuration of the CFF.

Because there are many joints, dramatically changing surfaces, and complex, narrow gaps, the hybrid grid system is employed in this study by applying the octree Cartesian grid for the surface and the background areas and the body-fit structured grid for the area near the wall. The surface grid distribution of the three-dimensional CFF and the grid distribution on the middle plane of the three-dimensional CFF calculation domain are shown in Figures 8a and 8b, respectively.

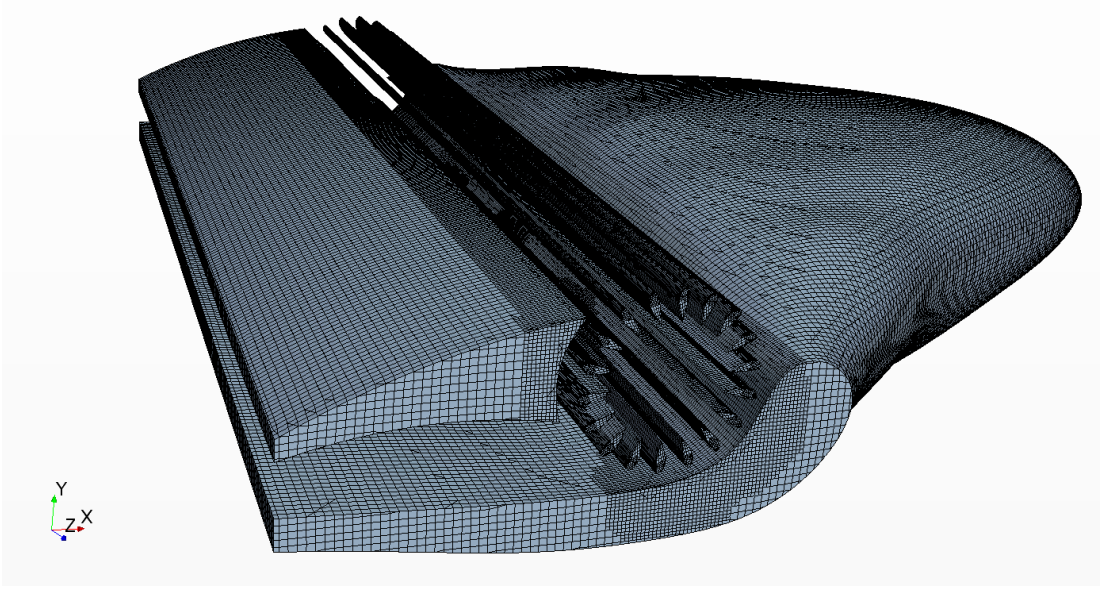

(**a**)

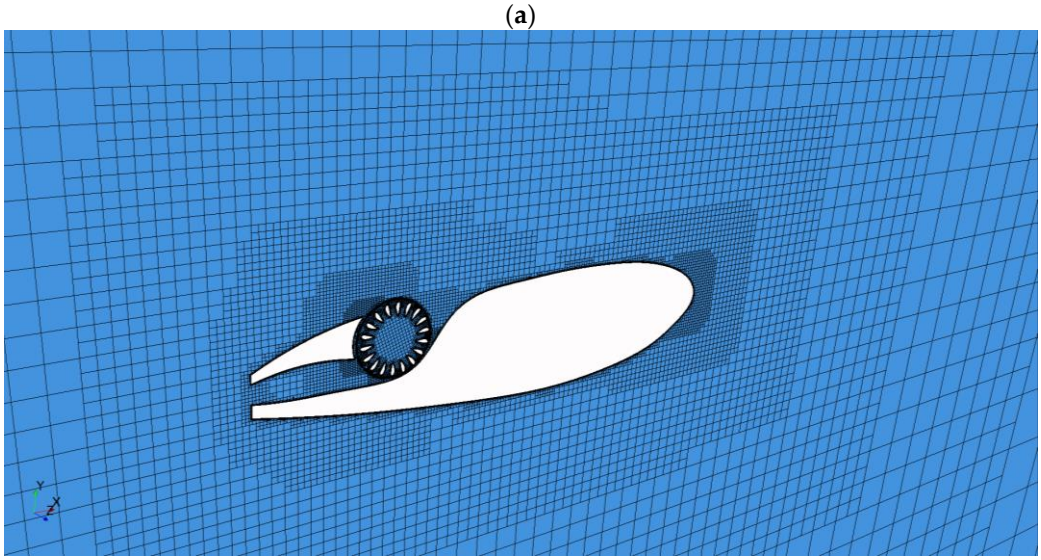

(**b**)

Figure 8. The grid system of the three-dimensional calculation domain: (**a**) surface grid distribution of the CFF; and (**b**) grid distribution on the middle plane of the three-dimensional CFF calculation domain.

The difficulties existing in simulations of a three-dimensional CFF root in the unsteady three-dimensional rotating boundary, the different physical phenomena that happened in the air and underwater, and the question of how to obtain the variation characteristics of the periodic flow. In this work, some typical CFD skills are correspondingly adopted to solve these problems. For instance, an initial flow field is achieved by steady calculation first and then is applied for the following unsteady situations. In addition, the unsteady forces and time are integrated and averaged with a user-defined field function.

Take the CFF operating in the air under conditions of the freestream velocity of 33.34 m/s, the angle of attack of 10°, and the rotating speed of 6000 rpm as an example to conduct the mesh-independent test. The corresponding numerical results are listed in Table 1. Three sets of the grid system, including the coarse grid, the fine grid, and the ultra-fine grid, and the corresponding performance are compared. It is found that the errors in the lift and the thrust between the fine grid and the ultra-fine grid are much smaller than those between the coarse grid and the ultra-fine grid. This means that both the fine grid and the ultra-fine grid are able to give rise to more reliable simulation results. Considering both the accuracy and efficiency of the numerical calculations, the optimal number of grids of

7.53×10^6 is ultimately selected for all the following numerical simulations. Normally, the computing duration of one typical numerical case study based on the fine grid is around 336 h by using a computer with a 3.6 GHz Inter 16 Processor and 32 GB RAM.

Table 1. Results of the mesh-independent test.

	Number of Grids	Lift/N	Error/%	Thrust/N	Error/%
Coarse grid	3.55×10^6	2940	3.95	240	5.14
Fine grid	7.53×10^6	3051	0.33	252	0.40
Ultra-fine grid	13.27×10^6	3061	-	253	-

4.1. CFF Operating in the Air

As for the numerical study of aerodynamic characteristics of a CFF operating in the air, the pressure p and the velocity V are respectively set as 101,325 Pa and 33.34 m/s, the angle of attack α ranges from 0° to 20°, and the rotating speed n ranges from 4000 to 8000 rpm. The velocity fields at different rotating speeds (n = 4000 rpm, n = 6000 rpm, n = 8000 rpm) under the condition of the same angle of attack of 10° are shown in Figure 9. It is found that:

(1) The air is suctioned by high-speed rotating blades and jetted to the tail of the body through the flow passage;
(2) The flow velocity around the blades is much higher than that in the rest of the regions; and
(3) The maximum velocity within the calculation domain increases with the increment of the rotating speed.

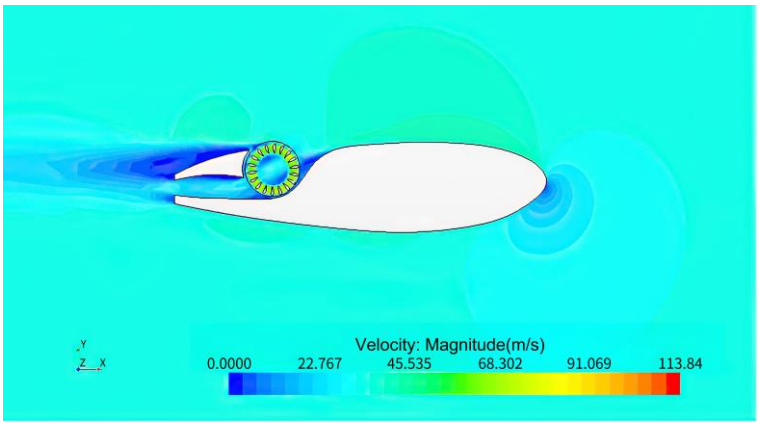

(**a**)

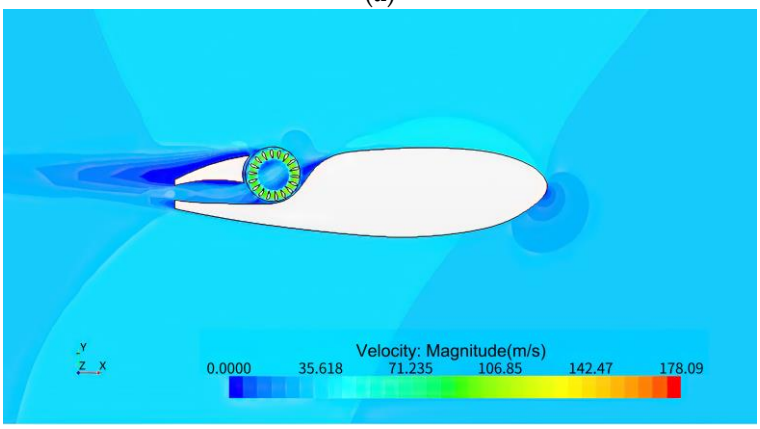

(**b**)

Figure 9. *Cont.*

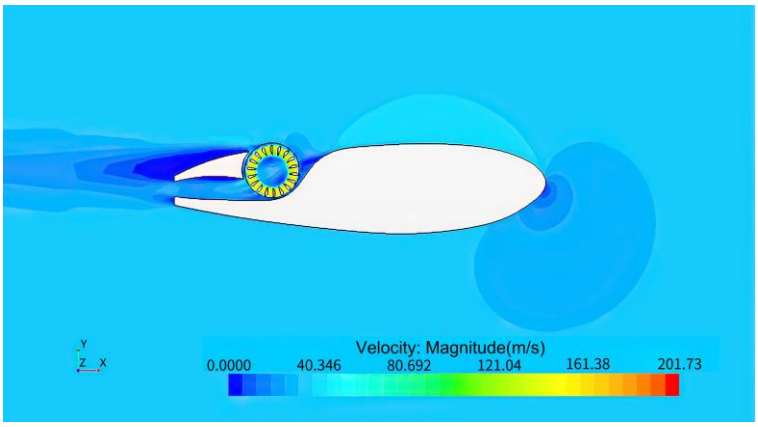

(**c**)

Figure 9. Velocity fields at different rotating speeds (α = 10°): (**a**) n = 4000 rpm; (**b**) n = 6000 rpm; and (**c**) n = 8000 rpm.

The variations of the lift and the thrust with the angle of attack and with the rotating speed are given in Figures 10a and 10b, respectively. Figure 10a shows that, at a given rotating speed of 6000 rpm, the lift increases with the increment of the angle of attack, while the thrust shows the opposite trend. Figure 10b displays that, at a given angle of attack of 10°, both the lift and the thrust grow with the increment of the rotating speed.

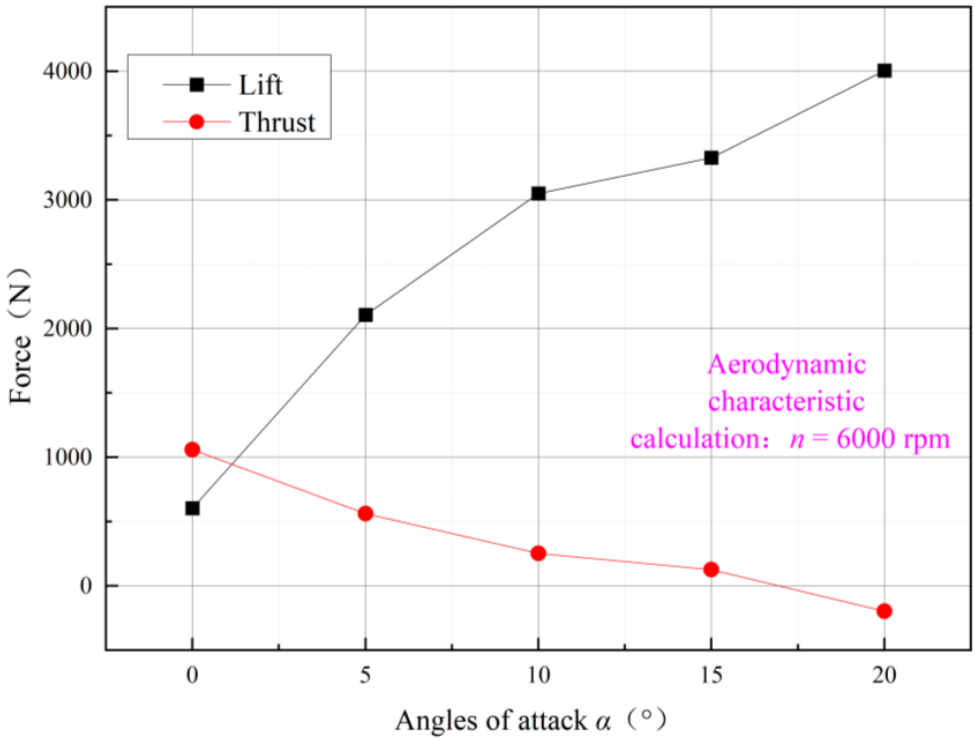

(**a**)

Figure 10. *Cont.*

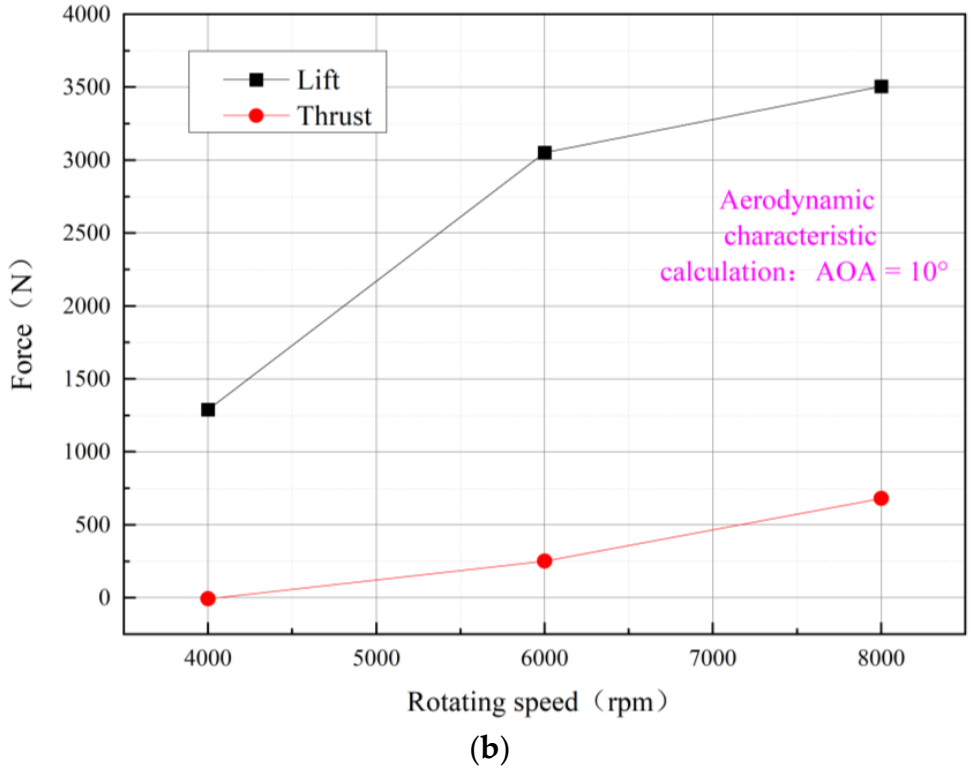

(**b**)

Figure 10. Variations of the lift and the thrust: (**a**) with the angle of attack; and (**b**) with the rotating speed.

In detail, as shown in Figure 10a, the thrust at the rotating speed of 6000 rpm almost linearly decreases with the increment of the angle of attack from 0° to 20°. The variation of the lift with increasing the angle of attack shows that there may be a critical angle of attack that causes the submersible aircraft to stall when increasing the angle of attack. In addition, the thrust decreases to a negative value when the angle of attack is larger than 15°. This is because the CFF has difficulty sucking enough air to generate positive thrust when the angle of attack is larger than 15°. Similarly in Figure 10b, the generated lift at the angle of attack of 10° greatly increases when the rotating speed increases from 4000 rpm to 6000 rpm but slows down after a rotating speed of 6000 rpm. This indicates that, at a certain angle of attack, there may also be a maximum lift. That is, no matter how much the rotating speed increases, the pressure difference between the upper and lower surfaces of the submersible aircraft does not change and the lift thus tends to be stable at a maximum value. Therefore, further investigation into the performance envelope of submersible aircraft is needed in future works.

4.2. CFF Operating Underwater

The high rotating speed of blades produces local cavitation when a CFF operates underwater [37], which dramatically induces unstable, irregular, and random changes in the lift and thrust and thus greatly affects the efficiency of the CFF. This is a fatal problem for the propeller of submersible aircraft. Figure 11 showed the local cavitation induced by a high rotating speed of 2000 rpm at given conditions of a pressure of 131,722 Pa, a velocity of 3.08 m/s, and an angle of attack of −10°. The cavitation mainly occurs in the regions of the fan center and around the edges of the blades where the flow speed is extremely high and the pressure is extremely low.

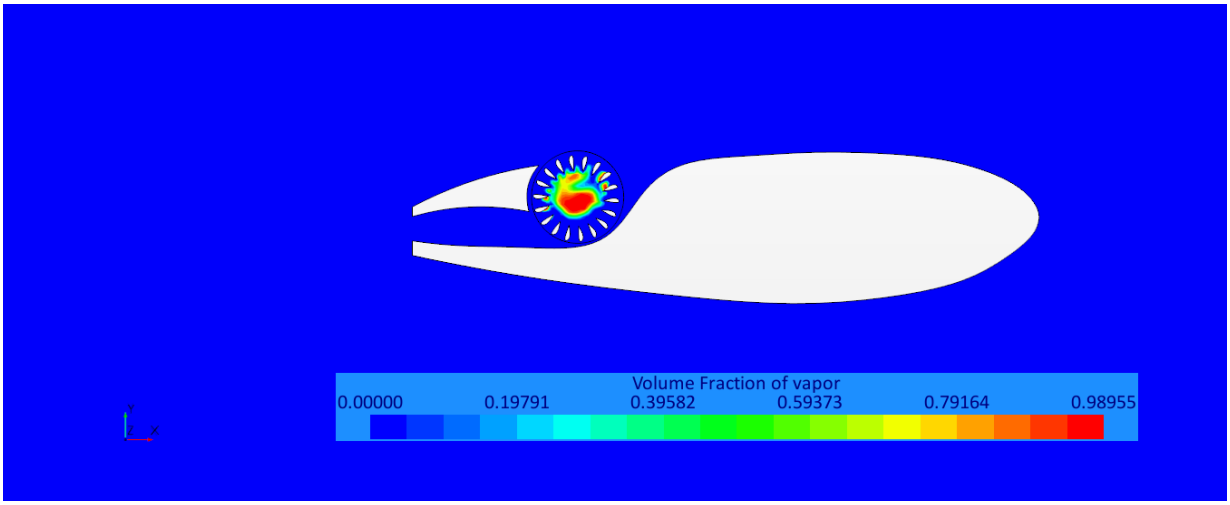

Figure 11. Local cavitation caused by a high rotating speed of 2000 rpm at given conditions of a pressure of 131,722 Pa, a velocity of 3.08 m/s, and an angle of attack of $-10°$.

Numerical studies show that the maximum rotating speed of a CFF effectively operating underwater is 1000 rpm. Taking the CFF operating at a rotating speed of 200 rpm as an example, the distribution of the corresponding pressure field is shown in Figure 12. The lowest pressure in this figure is obtained as 54,341 Pa, which is much higher than the critical cavitation pressure of 3450 Pa. Therefore, the low rotating speed of 200 rpm of a CFF operating underwater can successfully avoid the cavitation phenomenon.

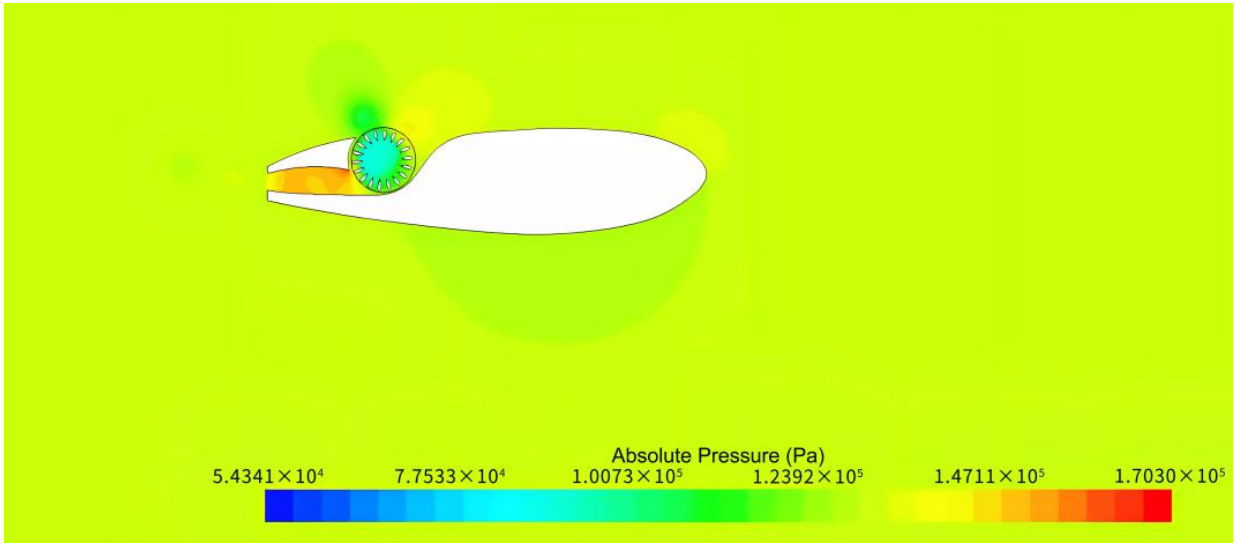

Figure 12. Pressure distribution at a low rotating speed of 200 rpm.

The conditions for the numerical study of hydrodynamic characteristics of a CFF operating underwater are given as p = 131,722 Pa, V = 3.08 m/s, angles of attack ranging from $-20°$ to $0°$, and rotating speeds ranging from 200 rpm to 1000 rpm. The variations of the lift and the thrust with the angle of attack and with the rotating speed are shown in Figures 13a and 13b, respectively.

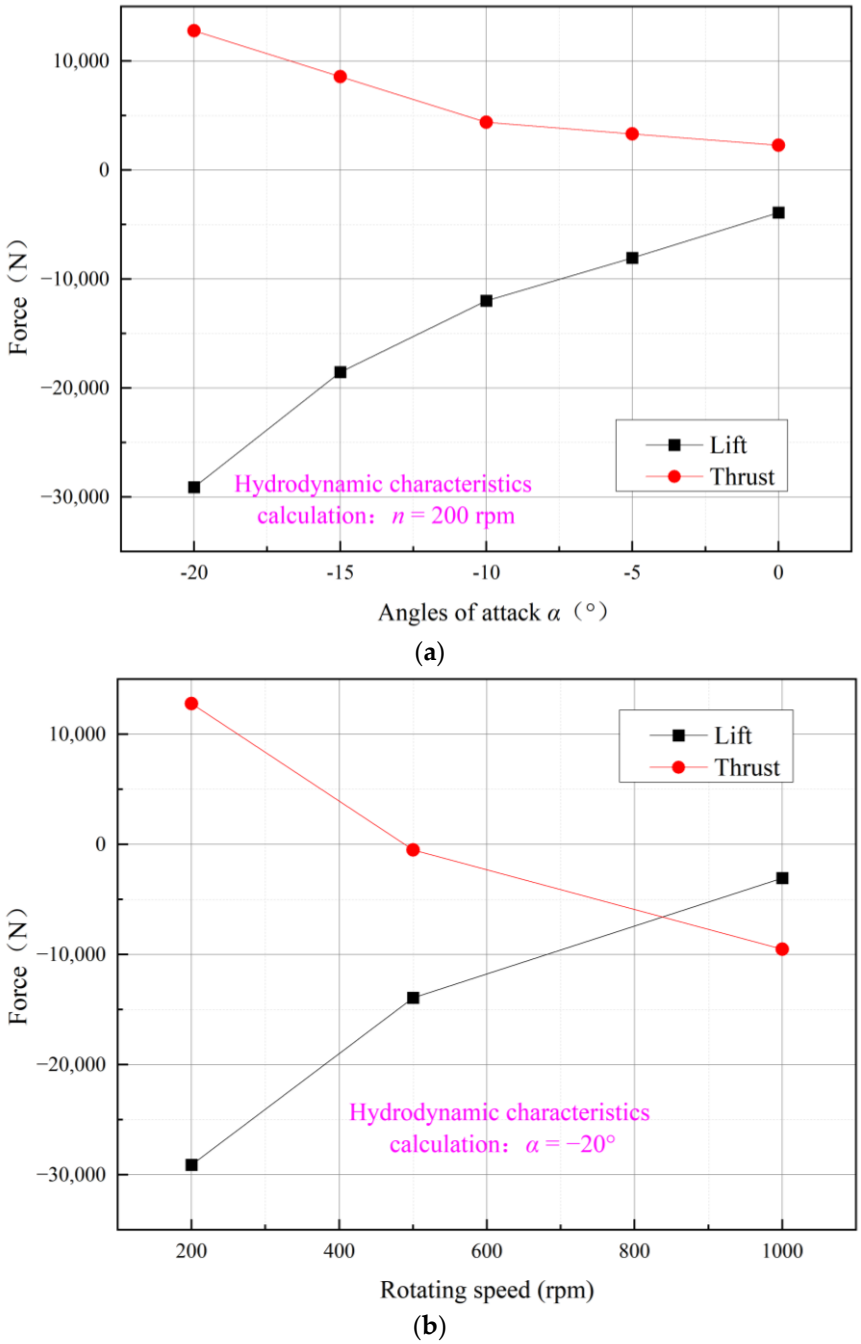

Figure 13. Variations of the lift and the thrust: (**a**) with the angle of attack; and (**b**) with the rotating speed.

It is seen from Figure 13a that, at a given rotating speed of 200 rpm, the lift increases with the increment of the angle of attack, while the thrust shows the opposite trend. The thrust always maintains at a positive value no matter how the angle of attack varies. This means that the submersible aircraft can always be propelled forward with the proposed CFF configuration at any angle of attack. The lifts with negative values mean that reasonable downward vertical forces can be properly generated by changing the angle of attack of the submersible aircraft. Take the velocity fields (Figure 14) at conditions of a given rotating speed of 500 rpm and angles of attack 0°, −5°, −10°, and −15° as examples. This shows that the influence of the angle of attack on the flow field at a given rotating speed is distinct. By decreasing the angle of attack from 0° to −15°, the relative orientation between the suction side of the CFF and the freestream velocity significantly varies, which leads to a more obvious pressure difference between the upper and lower surfaces of the submersible

aircraft. Thus, as shown in Figure 13a, an increasing overall downward vertical force, that is, the decreasing lift with a negative value, is ultimately induced to overcome the buoyancy of the submersible aircraft along with decreasing the angle of attack from 0° to −20°. Figure 13b demonstrates that, at a given angle of attack of −20°, the lift increases with the increment of the rotating speed. Since the lifts are of negative values, the increasing lift means the generated downward vertical force is weakened along with increasing the rotating speed. In addition, the thrust shows the opposite trend of that of the lift. It decreases with an increase in the rotating speed from 200 rpm to 1000 rpm and becomes a negative value at 500 rpm. This means that the submersible aircraft can be effectively propelled forward at a rotating speed ranging from 200 rpm to 500 rpm. Therefore, the submersible aircraft operating underwater with a rotating speed of 200 rpm and an angle of attack of −20° can achieve much more beneficial lift and thrust simultaneously. Meanwhile, negative thrusts induced by high rotating speeds ranging from 500 rpm to 1000 rpm can be reasonably utilized to brake the forward movement of the submersible aircraft.

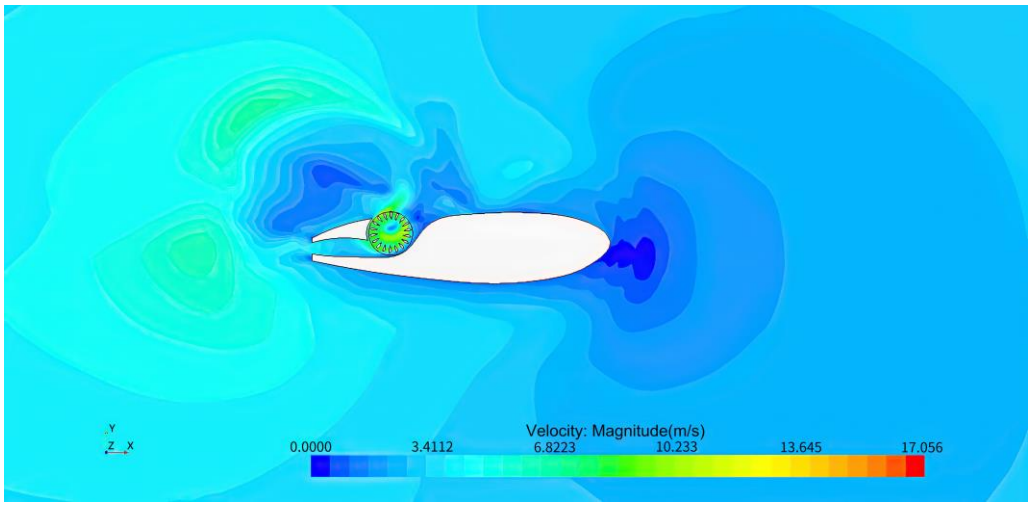

(**a**)

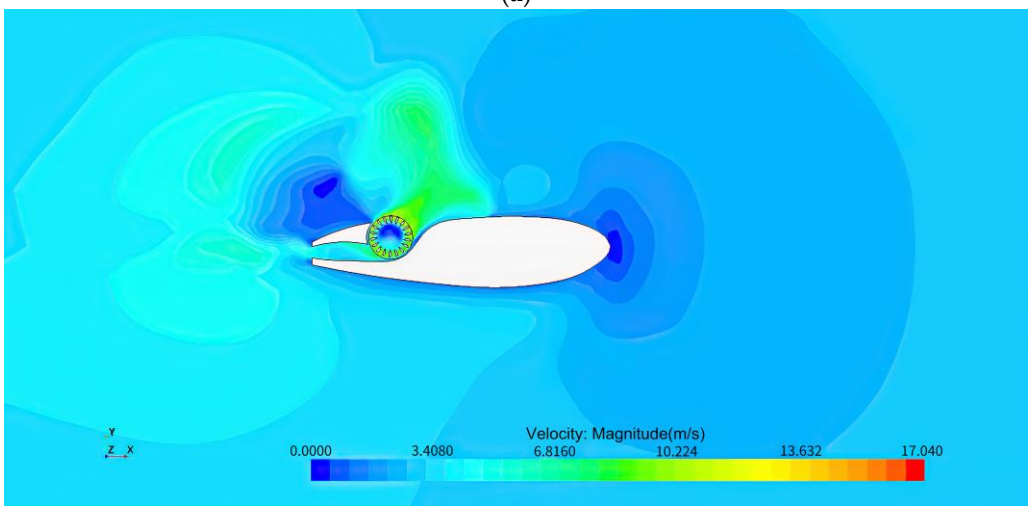

(**b**)

Figure 14. *Cont.*

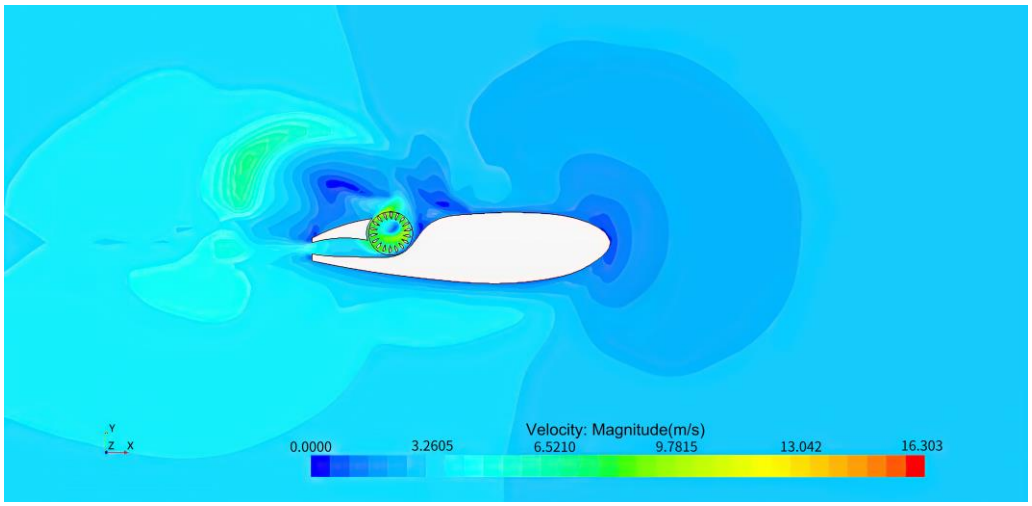

(**c**)

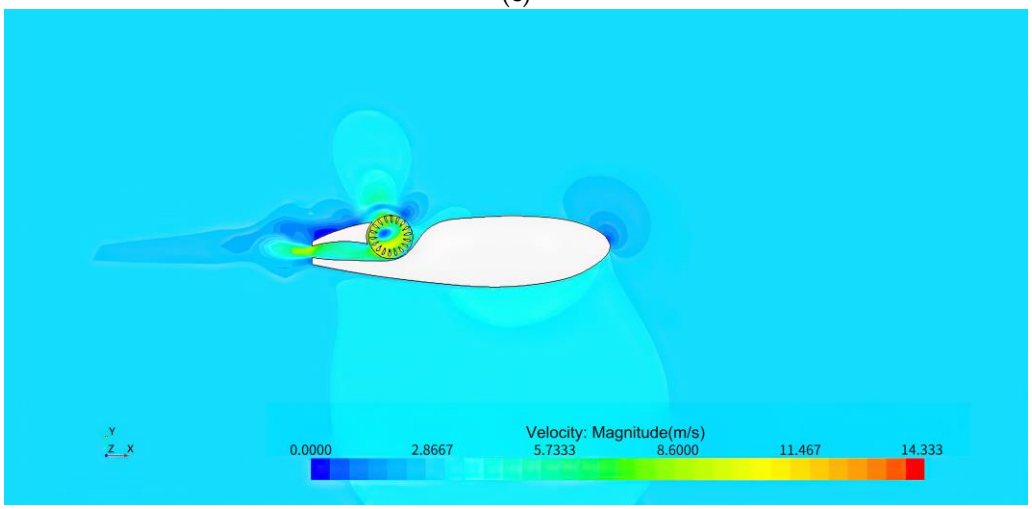

(**d**)

Figure 14. Velocity fields at different angles of attack ($n = 500$ rpm): (**a**) $\alpha = 0°$; (**b**) $\alpha = -5°$; (**c**) $\alpha = -10°$; and (**d**) $\alpha = -15°$.

Generally, the simulation results show that the CFF can be potentially applied as the general propulsion for submersible aircraft since reasonable lifts and thrusts are achieved both in the air and underwater. Essentially, at a given angle of attack, a high rotating speed is preferred to generate great lift and thrust for the CFF operating in the air, while a low rotating speed is desired to produce adequate lift and thrust simultaneously for the CFF operating underwater. At a given rotating speed, a large angle of attack can lead to high lift but also a high possibility of stalling and low thrust for the CFF operating in the air, while a small angle of attack is sufficient to produce both high thrust and high downward vertical force for the CFF operating underwater.

5. Conclusions

This work conducted a systematic numerical study on the different fluid dynamic characteristics of the CFF potentially applied in submersible aircraft. Numerical methodology is validated based on simulations of a two-dimensional CFF model. Based on the validated methodology, fluid dynamic characteristics of the three-dimensional CFF, including the velocity field, the pressure field, the cavitation distribution, the lift, and the thrust, are analyzed in depth. Results show the following: the proposed CFF can produce rational lifts and thrusts both in the air and underwater. Therefore, the CFF can be potentially applied as the general propulsion for submersible aircraft when the rotating speed and the

angle of attack are reasonably designed to meet the requirements of different application media. All the fluid dynamic characteristics of the CFF achieved in this work can provide a valuable reference for the future structural design of submersible aircraft. In addition to the current investigations, future works should focus on the characteristics of the water/air trans-media process of submersible aircraft.

Author Contributions: Numerical simulation, data analysis, and writing—original draft preparation, X.C.; writing—original draft preparation, C.Z.; data analysis, B.W. All authors have read and agreed to the published version of the manuscript.

Funding: This research received no external funding.

Institutional Review Board Statement: Not applicable.

Informed Consent Statement: Not applicable.

Data Availability Statement: Not applicable.

Acknowledgments: The authors thank the experts from the Key Laboratory of Hydrodynamics for their valuable opinions.

Conflicts of Interest: The authors declare no conflict of interest.

References

1. Goddard, R.; Eastgate, J. Submersible Aircraft Concept Design Study. In Proceedings of the 11th International Conference on Fast Sea Transportation, FAST, Honolulu, HI, USA, 26–29 September 2011.
2. Wang, Q.; Wu, S.; Hong, W.; Hong, W.; Zhuang, W.; Wei, Y. Submersible Unmanned Aerial Vehicle: Configuration Design and Analysis Based on Computational Fluid Dynamics. In Proceedings of the 3rd International Conference on Mechatronics and Mechanical Engineering (ICMME 2016), Shanghai, China, 21–23 October 2016.
3. Harloff, G.J. Cross Flow Fan Experimental Development and Finite Element Modeling. Ph.D. Thesis, University of Texas, Arlington, TX, USA, 1979.
4. Smith, L.H. Wake ingestion propulsion benefit. *J. Propul. Power* **1993**, *9*, 74–82. [CrossRef]
5. Roskam, J.; Lan, C.T.E. Airplane drag. In *Airplane Aerodynamics and Performance*; Design, Analysis and Research Corporation: Lawrence, KS, USA, 1997; pp. 137–199.
6. Kummer, J.; Dang, T. *Design and Simulation of an Embedded Cross-Flow Fan Propulsive Airfoil*; NASA Technical Report, Contract Number: NAS 303084; NASA: Washington, DC, USA, 2005.
7. Casparie, E.; Dang, T. High Lift/Low Drag Thick Subsonic Goldschmied/Griffith Airfoil with Integrated Cross-flow Fan Propulsion. In Proceedings of the International Powered Lift Conference, London, UK, 12–13 October 2008.
8. Peebles, P. Aerodynamic Lift Generating Device. U.S. Patent No. 6527229B1, 2003.
9. Gossett, D.H. Investigation of Cross-flow Fan Propulsion for Light Weight VTOL Aircraft. M.S. Thesis, Department of Mechanical & Aeronautical Engineering, Naval Postgraduate School, Monterey, CA, USA, 2000.
10. Yu, H.T. Experimental Investigation and Numerical Prediction of the Performance of a Cross-Flow Fan. M.S. Thesis, Naval Postgraduate School, Monterey, CA, USA, 2006.
11. Gao, T.; Lin, Y.; Ren, H. The role studies of fixed-wings in underwater fan-wing thrusters. *Ocean Eng.* **2020**, *216*, 108049. [CrossRef]
12. Benferhat, S.; Yahiaoui, T.; Imine, B.; Ladjedel, O.; Šikula, O. Experimental and numerical study of turbulent flow around a Fanwings profile. *Eng. Appl. Comput. Fluid Mech.* **2019**, *13*, 698–712. [CrossRef]
13. Seyfang, G.R. Fan Wing-Developments and Applications. In Proceedings of the 28th Congress of International Council of the Aeronautical Sciences, Brisbane, Australia, 23–28 September 2012.
14. Xiangnan, L. Research on the Aerodynamic Optimization of Design Parameters and Airfoil of Fanwing. M.S. Thesis, Nanjing University of Aeronautics and Astronautics, Nanjing, China, 2015.
15. Meng, L.; Ye, Y. Take-off characteristics and longitudinal controllability of Fan Wing. *Aircraft Eng. Aero. Technol.* **2016**, *88*, 783–790. [CrossRef]
16. Sun, K.; Ouyang, H.; Tian, J.; Wu, Y.; Du, Z. Experimental and numerical investigations on the eccentric vortex of the cross-flow fan. *Int. J. Refrig.* **2015**, *50*, 146–155. [CrossRef]
17. Duddempudi, D.; Yao, Y.; Edmondson, D.; Yao, J.; Curley, A. Computational study of flow over generic fan-wing airfoil. *Aircraft Eng. Aero. Technol.* **2007**, *79*, 238–244. [CrossRef]
18. Shojaeefard, M.H.; Askari, S. Experimental and numerical investigation of the flap application in an airfoil in combination with a cross flow fan. *Int. J. Numer. Methods Heat Fluid Flow* **2012**, *22*, 742–763. [CrossRef]
19. Askari, S.; Shojaeefard, M.H. Shape optimization of the airfoil comprising a cross flow fan. *Aircr. Eng. Aero. Technol.* **2009**, *81*, 407–415. [CrossRef]

20. Ahad, O.; Graham, J.M. Flight simulation and testing of the fan wing experimental aircraft. *Aircr. Eng. Aero. Technol.* **2007**, *79*, 131–136. [CrossRef]
21. Siliang, D.; Zhengfei, T. The aerodynamic behavioral study of tandem fan wing configuration. *Int. J. Aerosp. Eng.* **2018**, *2018*, 1594570. [CrossRef]
22. Siliang, D.; Zhengfei, T.; Pei, X.; Mengjiang, J. Study on helicopter antitorque device based on cross-flow fan technology. *Int. J. Aerosp. Eng.* **2016**, *2016 Pt 2*, 5396876.1–5396876.12. [CrossRef]
23. Gao, T.; Lin, Y.; Ren, H.; Tse, Z.T.H. Hydrodynamic analyses of an underwater fan-wing thruster in self-driving and towing experiments. *Measurement* **2020**, *165*, 108132. [CrossRef]
24. Wang, C.-N.; Yang, F.-C.; Nguyen, V.T.T.; Vo, N.T.M. CFD Analysis and optimum design for a centrifugal pump using an effectively artificial intelligent algorithm. *Micromachines* **2022**, *13*, 1208. [CrossRef]
25. Zhang, X.; Hu, C.; Tang, F.; Yang, F.; Song, X.; Liu, C.; Shi, L. Numerical and experimental study on the shutdown transition process of a large axial flow pump system focusing on the influence of gate control. *J. Mar. Sci. Eng.* **2023**, *11*, 280. [CrossRef]
26. Li, H.; Chen, Y.; Yang, Y.; Wang, S.; Bai, L.; Zhou, L. CFD simulation of centrifugal pump with different impeller blade trailing edges. *J. Mar. Sci. Eng.* **2023**, *11*, 402. [CrossRef]
27. Wilcox, D. *Turbulence Modeling for CFD*; DCW Industries, Inc.: La Canada, CA, USA, 1994.
28. Sauer, J.; Schnerr, G.H. Development of a new cavitation model based on bubble dynamics. *PMM-J. Appl. Math. Mec.* **2001**, *81*, 561–562. [CrossRef]
29. Magnus, R.J.; Yoshihara, H. Unsteady transonic flow over an airfoil. *AIAA J.* **1975**, *13*, 1622–1628. [CrossRef]
30. Jameson, A. Time-dependent Calculations Using Multigrid with Application to Unsteady Flows Past Airfoils and Wings. In Proceedings of the 10th Computational Fluid Dynamics Conference, Honolulu, HI, USA, 24–27 June 1991.
31. Pulliam, T.H. Time accuracy and the use of implicit methods. In Proceedings of the 11th Computational Fluid Dynamics Conference, Orlando, FL, USA, 6–9 July 1993.
32. Chen, Z.; Nguyen, V.; Choi, Y.D. Performance of an open ducted type very low head cross-flow turbine. In Proceedings of the Gmsarn International Conference, Ho Chi Minh City, Vietnam, 12–14 November 2014.
33. Li, Y.; Sun, D.; Meng, F.; Zheng, Y.; Zhong, Y. Study regarding the influence of blade rotation angle deviations on the hydraulic pulsation characteristics of a mixed-flow pump. *J. Mar. Sci. Eng.* **2023**, *11*, 530. [CrossRef]
34. Zhang, X.; Jiang, Y.; Song, X.; Tang, F.; Dai, J.; Yang, F.; Wang, H.; Shi, L. Investigation on the influence of flap valve area on transition process of large axial flow pump system. *J. Mar. Sci. Eng.* **2023**, *11*, 326. [CrossRef]
35. Chen, J.; Mao, J.; Shi, H.; Wang, X. Experimental and numerical study on the hydraulic characteristics of an S-type bidirectional shaft tubular pump. *J. Mar. Sci. Eng.* **2022**, *10*, 671. [CrossRef]
36. Dygert, R.K.; Dang, T.Q. Experimental Investigation of Embedded Cross-Flow Fan for Airfoil Propulsion/Circulation Control. In Proceedings of the 45th AIAA Aerospace Sciences Meeting and Exhibit, Reno, NV, USA; 2007.
37. Liu, H.; Tang, F.; Shi, L.; Dai, L.; Shen, J.; Liu, J. The analysis of cavitation flow and pressure pulsation of bi-directional pump. *J. Mar. Sci. Eng.* **2023**, *11*, 268. [CrossRef]